



PERGAMON

Available online at [www.sciencedirect.com](http://www.sciencedirect.com)

SCIENCE @ DIRECT®

Vision Research 43 (2003) 2861–2873

Vision  
Research

[www.elsevier.com/locate/visres](http://www.elsevier.com/locate/visres)

# Spatial and temporal tuning of motion in depth

Martin Lages \*, Pascal Mamassian, Erich W. Graf

*Department of Psychology, University of Glasgow, 58 Hillhead Street, Glasgow, G12 8QB Scotland, UK*

Received 15 May 2003; received in revised form 22 July 2003

## Abstract

We used the Pulfrich effect to investigate perception of motion in depth. Independent manipulation of spatial and temporal frequency content in stereoscopic motion stimuli revealed the tuning characteristics of motion-in-depth perception. Sensitivity to interocular phase difference between sinusoidally oscillating sine-wave gratings was measured in four observers who judged direction of motion in depth. Discrimination thresholds in terms of interocular phase difference were determined to investigate spatial and temporal tuning characteristics of a system that is based on interocular phase difference, interocular delay, binocular disparity and velocity difference. Temporal frequency tuning of interocular phase difference thresholds was band pass and relatively dependent on spatial frequency variation. These results together with evidence from two control experiments support the idea that sensitivity to direction of motion in depth is limited by a stereo-motion system that monitors binocular horizontal disparity and motion rather than interocular phase difference, interocular delay, or interocular velocity difference.

© 2003 Elsevier Ltd. All rights reserved.

*Keywords:* Pulfrich effect; Binocular disparity; Interocular delay; Interocular phase difference; Velocity difference

## 1. Introduction

Integration of motion and stereoscopic depth information is essential for the perception of dynamic events in a 3-D environment. Motion and stereo share a similar geometry to infer the distance between an object and the observer. Multiple images are in both cases used to triangulate the object's features, either over time or across eyes. Therefore, it is natural to expect that the neural structures involved in motion and stereo processing overlap.

From neurophysiological studies, it is well established that both direction and disparity selectivity appear as early as the primary visual cortex V1 (Hubel & Wiesel, 1968; Poggio & Fischer, 1977). Neurons in V1 project to middle temporal area MT where almost all neurons are directionally selective (Albright, 1984) and several areas throughout the visual cortex have neurons tuned to opponent motion (e.g., Pettigrew, 1973; Poggio & Fischer, 1977; Poggio & Talbot, 1981) as well as motion in depth (Cynader & Regan, 1978, 1982). Poggio and Talbot (1981) found cells in V1 and V2 and Maunsell

and Van Essen (1983) in MT that were tuned to a fixed disparity that, interestingly, was not necessarily the optimal disparity for motion in depth. There is evidence that binocular cells in mammalian visual cortex may process motion and depth together (Felleman & Van Essen, 1987). More recently, it was shown that binocular complex cells in the striate cortex of anesthetized cats (Anzai, Ohzawa, & Freeman, 2001) and cells in V1 and MT of alert monkeys (Pack, Born, & Livingstone, 2003) exhibit space–time oriented response profiles for interocular spatial–temporal shifts.

While neurophysiological evidence suggests close links between motion and disparity processing, the majority of psychophysical studies have investigated motion and binocular disparity separately. Accordingly, standard models of stereopsis are based on spatial considerations and disregard temporal aspects of depth perception (e.g., Fleet, Wagner, & Heeger, 1996; Ohzawa, 1998; Sanger, 1988) whereas classical models of motion detection ignore binocular input (Adelson & Bergen, 1985; Marr & Ullman, 1981; Reichardt, 1961; Van Santen & Sperling, 1985; Watson & Ahumada, 1985).

The present psychophysical study investigates characteristics of a possible motion-in-depth system by using the Pulfrich effect, a well-known stereo-motion

\* Corresponding author. Tel.: +44-141-330-6842; fax: +44-141-330-4606.

*E-mail address:* [m.lages@psy.gla.ac.uk](mailto:m.lages@psy.gla.ac.uk) (M. Lages).

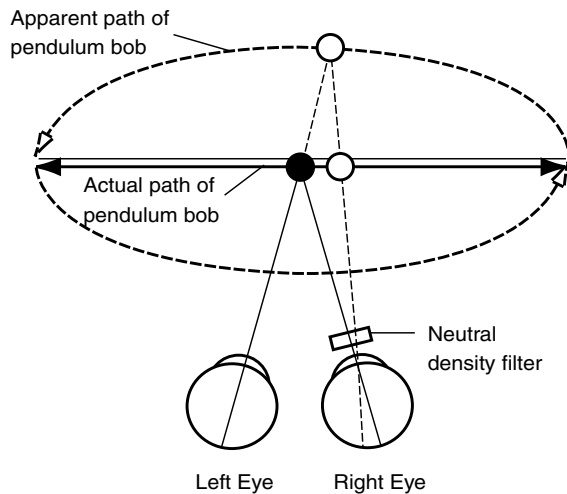


Fig. 1. Illustration of the classical Pulfrich effect in top view. A stimulus is oscillating in the frontal plane with eyes fixated straight ahead. If a neutral density filter is placed over the right eye the stimulus appears to rotate counter-clockwise in depth on an elliptical path. The temporal delay corresponds to a lateral displacement of the stimulus in turn introducing a binocular disparity. Due to the geometry of the effect the actual path of the pendulum does not coincide with the major axis of the elliptical path.

phenomenon. The Pulfrich effect and variants of it have intrigued vision researchers for decades (see Howard & Rogers, 2002, chapter 28). The classical phenomenon<sup>1</sup> refers to the observation that an object oscillating back and forth in the frontal plane appears to move along an elliptical path in depth when a neutral density filter is placed in front of one of the eyes (Pulfrich, 1922). The illustration in Fig. 1 provides an informal sketch of the phenomenon.

Three main explanations of the Pulfrich effect have been put forward.

- (1) The classical explanation of this phenomenon relates to the idea that the neutral density filter induces an interocular temporal delay in neuronal transmission. There is considerable evidence supporting this assumption (e.g., Carney, Paradiso, & Freeman, 1989; Julesz & White, 1969; Rogers & Anstis, 1972). The delay then corresponds to a spatial displacement of the stimulus that is interpreted

<sup>1</sup> Pulfrich first demonstrated the stereo-motion illusion using a stimulus that did not describe simple harmonic motion. He designed an apparatus with a stationary lower pointer and a moving upper pointer vertically aligned in the center of a square aperture. The upper pointer was one of six pointers mounted on an axis similar to spokes on a wheel. The axis was positioned above the aperture and occluded from view. When the axis turned the upper pointer rotated out of the aperture to be replaced by the next pointer. In a second apparatus he demonstrated that motion in depth can be reduced to horizontal harmonic motion using vertical pointers mounted on a horizontal disk (Pulfrich, 1922).

as horizontal disparity between the eyes. Hence, interocular delay creates spatial disparity leading to the perception of motion in depth (Pulfrich, 1922).

- (2) An alternative explanation is based on the assumption that interocular delay alone can be used to extract depth information. Pulfrich-like effects have been observed in dynamic random-dot patterns (e.g., Burr & Ross, 1979; Falk, 1980; Morgan & Ward, 1980; Norcia & Tyler, 1984; Ross, 1974; Tyler, 1974), stroboscopic stimuli (e.g., Burr & Ross, 1979; Lee, 1970; Morgan, 1975, 1979; Morgan & Thompson, 1975; Ross & Hogben, 1975), as well as binocularly uncorrelated random-dot patterns (Shioiri, Saisho, & Yaguchi, 2000). The results of these experiments suggest that neither horizontal disparity nor coherent motion is a pre-requisite for the perception of motion in depth and promote the idea that interocular temporal delay provides an independent depth cue.
- (3) There is a third explanation that can encompass the previous ones. The visual system may process binocular horizontal disparity and interocular delay simultaneously (Burr & Ross, 1979; Morgan, 1979; Qian, 1994; Qian & Andersen, 1997). Recent physiological evidence in cat and monkey supports the view that disparity and motion are jointly encoded by binocular cells in area V1 (Anzai et al., 2001; Pack et al., 2003) before further stereo-motion processing occurs in extrastriate cortical areas (Cynader & Regan, 1978, 1982; Felleman & Van Essen, 1987).

The three explanations are illustrated in Fig. 2. The space–time plot depicts sinusoidal motion of the stimulus with a temporal phase shift between left and right eye. Each of the three alignments between sinusoidal motion in the left and right eye represents a potential input for stereoscopic motion processing: (1) binocular horizontal disparity  $H$ , (2) interocular delay  $T$ , and (3) interocular space–time offset (disparity–delay). Clearly, disparity and delay are special cases of all possible interocular space–time offsets. Fig. 2 also illustrates that various detectors differently oriented in disparity and time can solve the correspondence problem for motion in depth.

Most psychophysical studies on the Pulfrich effect have tried to disambiguate horizontal disparity from interocular delay and to design the ultimate stimulus that would shed light on one or the other mechanism underlying the effect. While these studies provided important data to understand the phenomenon, they eventually lack generality. In the present study, we take a different approach by looking at the spatial and temporal tuning characteristics of a stimulus that moves directionally in depth. Spatial and temporal tuning of motion in the fronto-parallel plane is well documented

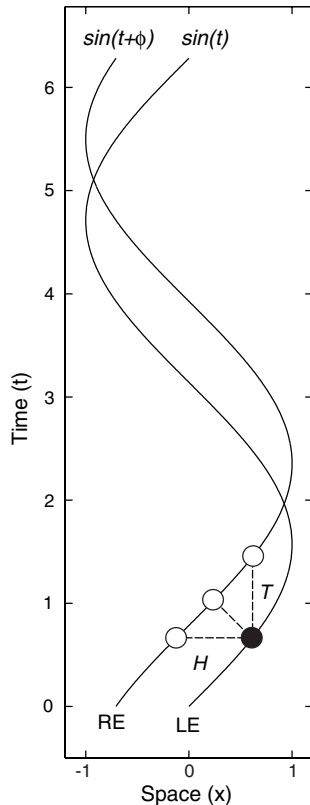


Fig. 2. Space–time plot of sinusoidal motion in the left and right eye. Introducing a phase difference of  $\phi$  by placing a neutral density filter over the right eye corresponds to (1) a horizontal disparity  $H$ , (2) an interocular temporal delay  $T$ , and (3) an interocular space–time offset. Note that (1) and (2) are special cases of (3).

but very few studies have systematically addressed spatial and temporal aspects of motion in depth.<sup>2</sup> One difficulty in previous studies is the lack of control over spatial frequency content. Thresholds for motion in depth are based on moving dots (e.g., Burr & Ross, 1979), moving lines and bars (e.g., Regan & Beverley, 1973a, 1979; Tyler, 1971), moving random-dot stereograms (e.g., Beverley & Regan, 1974; Julesz & White, 1969; Lu & Sperling, 1995; Regan & Beverley, 1973b), and flickering random patterns (Morgan & Fahle, 2000). These stimuli are broad band in spatial frequency and contain many velocity components even if temporal frequency is held constant. Therefore it remains unclear whether tuning characteristics are due to temporal frequency or velocity content in the images.

Another critical problem with previous studies is that the observer can often perform the task by attending to fronto-parallel motion direction or disparity information alone. In a typical motion-in-depth detection task, for example, a stimulus oscillates in the medial plane of the head, towards and away from the observer. Perform-

mance in such a task can be based on detection of opposite fronto-parallel motion in the left and right eye or static disparity differences at inflection points but not necessarily on the perception of motion in depth.

Here we designed a task in which observers had to discriminate motion direction in depth to give a correct response. In a variant of the Pulfrich phenomenon we manipulated the phase difference between sinusoidal motion in the left and right eye to determine thresholds for the discrimination of clockwise and counter-clockwise rotation in depth. Independent control over spatial and temporal frequency of the stimulus can reveal tuning characteristics that will help us to differentiate between explanations of the Pulfrich effect and related models of motion-in-depth processing.

## 2. Experiment

We recreated the Pulfrich phenomenon using sine-wave gratings moving within a stationary Gaussian spatial envelope. This stimulus offers independent control over spatial and temporal frequency content. The sinusoidal carriers in the left and right eye were offset by a small phase difference so as to produce the impression of a periodic motion in depth. The profiles of the sinusoidal carriers are described in Eq. (1)

$$\begin{aligned} C_l(x, t) &= \cos\{\omega_x x + \sin(\omega_t t + \phi/2)\}, \\ C_r(x, t) &= \cos\{\omega_x x + \sin(\omega_t t - \phi/2)\}, \end{aligned} \quad (1)$$

where  $\omega_x$  is the angular spatial frequency (measured in radians per degree visual angle),  $\omega_t$  the angular temporal frequency (in rad/s), and  $\phi$  the phase difference between the two eyes.

The phase difference was systematically varied across trials and observers had to report ‘clockwise’ or ‘counter-clockwise’ direction of motion in depth. It is important to note that in this task neither disparity sign alone nor motion direction alone is sufficient for a correct response. For instance, to correctly perceive a grating rotating clockwise in depth, the observer will have to associate leftward motion with crossed disparities (in front of fixation) and rightward motion with uncrossed disparities.

This stimulus has the following general properties (see Appendix A for details):

- (1) *Interocular phase difference* (see Appendix A.1): An interocular delay is produced by introducing an interocular phase difference  $\Delta\phi$  (expressed in radians) between the sinusoidal oscillations in the left and right carrier

$$\Delta\phi = +\phi/2 - (-\phi/2) = \phi. \quad (2)$$

The interocular phase difference is also a good approximation of the maximal spatial phase difference

<sup>2</sup> In the following we use the term “motion in depth” to describe any motion trajectory in 3-D space.

(see Appendix A.3). Kaufman and Palmer (1990) found that attenuating the luminance by placing a neutral density filter over one eye causes a temporal stretching rather than a pure delay in the response of simple cells. Introducing a constant interocular phase difference rather than using a neutral density filter therefore avoids the issue of temporal stretching.

- (2) *Interocular delay* (see Appendix A.2): In each trial a given interocular phase difference corresponds to a fixed interocular delay  $T$  (expressed in seconds)

$$T = \frac{\phi}{\omega_t}. \quad (3)$$

- (3) *Binocular horizontal disparity* (see Appendix A.3): In each trial, horizontal disparities vary sinusoidally in time with temporal frequency  $\omega_t$ . Disparity therefore depends on both spatial and temporal frequencies (see also Fig. 6 in Appendix). Maximal horizontal disparity  $H_{\max}$  (expressed in arcsec of visual angle) is well approximated by

$$H_{\max} \approx \frac{\phi}{\omega_x}. \quad (4)$$

- (4) *Interocular velocity difference* (see Appendix A.4): In each trial the left and right images move sinusoidally over time such that velocity varies between  $\pm\omega_t/\omega_x$ .

Maximal interocular velocity difference is expressed in deg/s and is well approximated by

$$U_{\max} \approx \phi \frac{\omega_t}{\omega_x}. \quad (5)$$

Note that maximal interocular velocity difference is the same as maximal change in horizontal disparity.

By examining the tuning characteristics for spatial and temporal frequency variation, we can test whether discrimination performance is best described by a system that is based on interocular phase difference (spatial–temporal offset), interocular delay, (maximal) horizontal disparity, or (maximal) interocular velocity difference. The resulting tuning predictions are illustrated in Fig. 3A–D with interocular phase thresholds plotted against temporal frequency for each spatial frequency condition. These predictions are summarised below:

- (1) A motion-in-depth system based on interocular phase difference should produce constant thresholds independent of spatial and temporal frequency variation as shown in Fig. 3A.
- (2) A system that monitors interocular delay should be independent of spatial frequency but dependent on temporal frequency variation as illustrated in Fig. 3B.

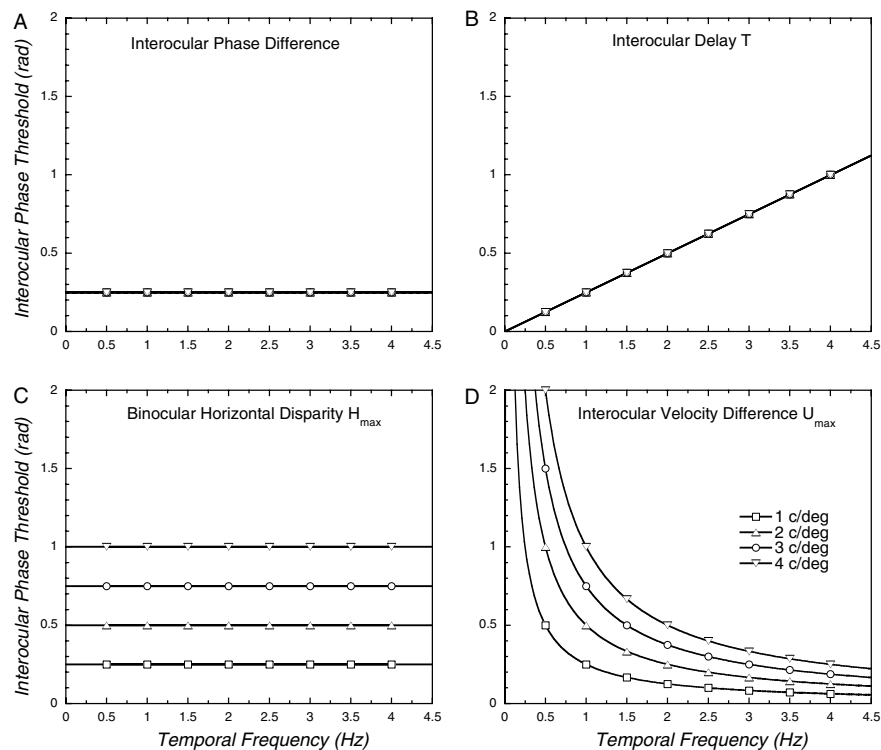


Fig. 3. Prediction of tuning functions for different inputs. Interocular phase thresholds are plotted against temporal frequency (0.5–4.5 Hz) for different spatial frequencies (1–4 c/deg). Panel A describes tuning functions for interocular phase difference, B for interocular delay, C for binocular horizontal disparity, and D for interocular velocity difference. Tuning functions shift vertically, horizontally or change in curvature as a result of spatial and temporal frequency variation in the stimulus (see text for explanation).

- (3) If a motion-in-depth system monitors horizontal disparity then discrimination performance is limited by maximal horizontal disparity in the stimulus. Thus, performance measured by interocular phase thresholds should be independent of temporal frequency but dependent on spatial frequency variation as illustrated in Fig. 3C.
- (4) Finally, if a motion-in-depth system is based on interocular velocity difference then discrimination performance is limited by maximal velocity difference in the stimulus. Thus, interocular phase thresholds should depend on spatial and temporal frequency as shown in Fig. 3D.

Of course, the first three predictions are incomplete because a model that monitors only interocular phase difference, interocular delay or maximal horizontal disparity would perform at chance level in our discrimination task. Nevertheless, we include these predictions to give the reader an intuition of the possible impact of each of these attributes on the final thresholds.

### 3. Methods

#### 3.1. Stimuli

We recreated the Pulfrich phenomenon using carriers moving within a Gaussian spatial envelope. The carriers were sinusoidally moving, vertically oriented sine-wave gratings presented binocularly. The intensity of the left and right images can be described as

$$\begin{aligned}
 I_l(x, y, t) &= L_0[1 + M \cos\{\omega_x x + \sin(\omega_t t + \phi/2)\} \\
 &\quad \times \exp\{-(x^2 + y^2)/2\sigma^2\}], \\
 I_r(x, y, t) &= L_0[1 + M \cos\{\omega_x x + \sin(\omega_t t - \phi/2)\} \\
 &\quad \times \exp\{-(x^2 + y^2)/2\sigma^2\}],
 \end{aligned}
 \tag{6}$$

where  $\sigma$  denotes the width of the spatial envelope, and  $\omega_x$ ,  $\omega_t$  and  $\phi$  are defined as in Eq. (1). All stimuli had a mean luminance of  $L_0 = 34$  cd/m<sup>2</sup> with Michelson contrast  $M = (L_{\max} - L_{\min})/(L_{\max} + L_{\min}) = 0.1$ . Vertical gratings were displayed in circular Gaussian spatial envelopes ( $\sigma = 0.69$  deg or 35 pixels) for 1 s. Stimuli subtended 4.0 deg visual angle (210 by 210 pixels) and were centered 4.76 deg above the 0.57 deg fixation cross (30 by 30 pixels).

Across sessions we systematically varied temporal frequency  $\omega_t$  of sinusoidal oscillation and spatial frequency  $\omega_x$  of the oscillating carrier. Temporal frequencies were set to 0.25 Hz and between 0.5 and 5.0 Hz at intervals of 0.5 Hz. Spatial frequency ranged from 1 to 4 cycles per degree visual angle (c/deg) in steps of 1 c/deg. Phase difference varied between  $-\pi/4$  and  $+\pi/4$  at intervals of  $\pi/14$ . Direction of sinusoidal motion (i.e., sign

of phase difference), interocular phase difference, and initial phase of the carrier were randomised across trials.

For a presentation time of 1 s, the number of stimulus oscillations corresponds to the temporal frequency of sinusoidal motion. In order to display at least half a cycle of the elliptical path in depth, presentation time was increased to 2 s in the 0.25 Hz condition only.

#### 3.2. Apparatus

The task was programmed in MatLab using the Psychophysics Toolbox extensions (Brainard, 1997; Pelli, 1997) and run on a Macintosh G4 Dual 500 MHz computer with a 21 inch Sony GDM-F500R cathode-ray tube flat screen monitor. The monitor was calibrated for luminance using a Minolta Chroma Meter CS-100. Stimuli were presented in a split-screen Wheatstone configuration at a viewing distance of 114 cm with a frame rate of 120 Hz. Observers were seated in front of haploscopic mirrors with their head supported by a chin- and headrest. The experimental room was dimly lit by the monitor display.

#### 3.3. Observers

Four observers with experience in psychophysical tasks took part, two of them (WA and JW) were naïve as to the objectives of the experiment and two were authors (EG and ML). Observer EG had normal visual acuity and observers ML, WA, and JW had corrected-to-normal visual acuity. All observers had good stereo vision.

#### 3.4. Procedure

Thresholds for the discrimination of motion direction in depth were measured by the method of constant stimuli. Observers judged direction of motion in depth, i.e. clockwise or counter-clockwise motion when the scene is imagined from above. With 10 temporal and four spatial frequency conditions each observer attended forty sessions over several days. Observer JW had two additional temporal frequency conditions leading to 48 sessions in total.

Each session lasted approximately 20 min and was structured as follows: (1) A fixation-cross flanked by nonius lines was presented in stereoscopic view. (2) When the fixation cross was seen in perfect alignment with the nonius lines the participant initiated the first trial by key press. (3) An interval of 0.5 s followed. (4) Moving sine-wave gratings in a spatial envelope were presented for 1.0 s (2.0 sec at 0.25 Hz) above the fixation cross in stereoscopic view. (5) When the participant responded the next trial commenced with the presentation of the fixation cross followed by another test grating randomly drawn from a set of eight phase differences,

and two directions of motion in depth. The observer's task was to indicate direction of motion in depth (clockwise or counter-clockwise from a bird's eye view) by pressing labeled keys. No feedback was given. Eight repetitions for eight phase differences and two motion directions gave a total of 128 trials per condition. Collapsing the data over equivalent combinations of motion direction and phase difference gave 16 observations per data point.

### 3.5. Psychometric function

A Gaussian cumulative distribution function  $G(x; \mu, \sigma)$  was fitted to the data of each subject and condition using a constrained maximum likelihood fit (Wichmann & Hill, 2001a). The psychometric function  $\Psi(x)$  is described by four parameters

$$\Psi(x; \mu, \sigma, \gamma, \lambda) = \gamma + (1 - \gamma - \lambda) \cdot G(x; \mu, \sigma). \quad (7)$$

The mean  $\mu$  and the standard deviation  $\sigma$  correspond to the 50% point and the difference between 50% and 84.1% point of the Gaussian cumulative distribution function, respectively. The estimates of parameter  $\gamma$  and  $\lambda$  were constrained to values between 0 and 0.05 and refer to a limited "guess rate" and "miss rate", respectively. If no response bias is present parameter  $\mu$  coincides with a phase difference of zero and  $\sigma$  is taken as the discrimination threshold for motion direction in depth. Confidence intervals of parameter estimates were determined by a parametric bootstrapping technique (Wichmann & Hill, 2001b). The method of percentiles was applied and  $\pm 1$  standard deviation of 999 simulations was used as confidence interval for the discrimination threshold.

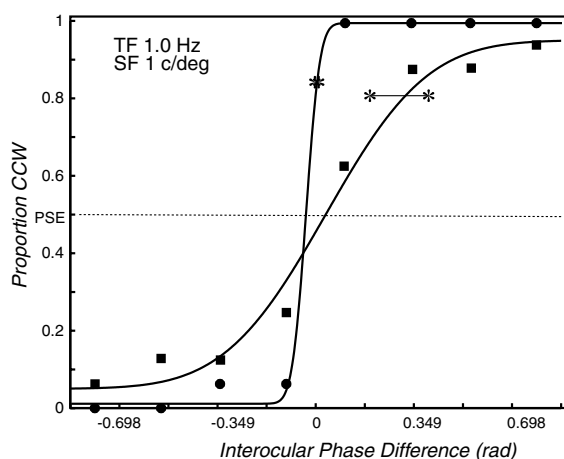


Fig. 4. Psychometric functions (continuous lines) fitted to data of best (circles) and worst (squares) discrimination performance. Interocular phase difference (rad) is plotted against proportion of 'counter-clockwise' (CCW) responses for vertical gratings of 1 c/deg oscillating horizontally at 1.0 Hz. Stars denote confidence intervals of discrimination thresholds ( $\pm 1$  standard deviation of simulated data at 84.1% point corrected for estimated guess and miss rate).

Two examples of individual performances in this discrimination task are shown in Fig. 4. Psychometric functions are fitted to the data of the best (WA) and worst (ML) performance at 1 Hz and 1 c/deg. As the magnitude of the phase difference changes, the proportion of counter-clockwise (CCW) responses increases from zero to one. A small discrimination threshold therefore indicates high sensitivity for direction of motion in depth. Discrimination thresholds beyond  $2\pi/3 = 2.09$  (120 deg phase angle) were not considered as they reflect nearly random performance and a poor fit of the psychometric function.

## 4. Results

Similar to the classical Pulfrich illusion, the carrier within the Gaussian window appeared to move smoothly on an elliptical path in depth. An increase in phase difference resulted in the perception of the grating travelling on an elliptical path extended in depth. If the phase difference was too small, the grating appeared to oscillate left and right in the frontal plane and the observer had to guess direction of motion in depth. When the phase difference was negative the grating appeared to rotate in the opposite direction in depth. The circumference of the path scaled with spatial frequency.

Discrimination thresholds for perceiving direction of motion in depth varied considerably between observers when individual discrimination thresholds are plotted against temporal frequency as shown in Fig. 5. Across observers and conditions lowest interocular phase thresholds varied tenfold between 0.023 and 0.228 rad. Alternatively, these interocular phase thresholds can be expressed in terms of interocular delay, maximal horizontal disparity, and maximal velocity difference. Lowest delay thresholds ranged between 1.4 and 24.3 ms, lowest disparity thresholds varied between 4.8" and 68.2" and lowest velocity difference thresholds between 0.3 and 3.1 deg/s. Note that large individual differences are commonly observed in phenomena involving stereopsis (e.g., Howard & Rogers, 2002).

### 4.1. Tuning functions

Interocular phase thresholds followed a U-shape curve when they are plotted against temporal frequency, thus indicating a band-pass mechanism (see Fig. 5). The peak performances were extracted by fitting parabolas to phase thresholds:

$$y = a(x - b)^2 + c, \quad (8)$$

where parameter  $a$  is the half-curvature,  $b$  represents a horizontal shift, and  $c$  a vertical shift. Discrimination thresholds were fitted (in the maximum likelihood sense) for each observer in each of the four spatial frequency

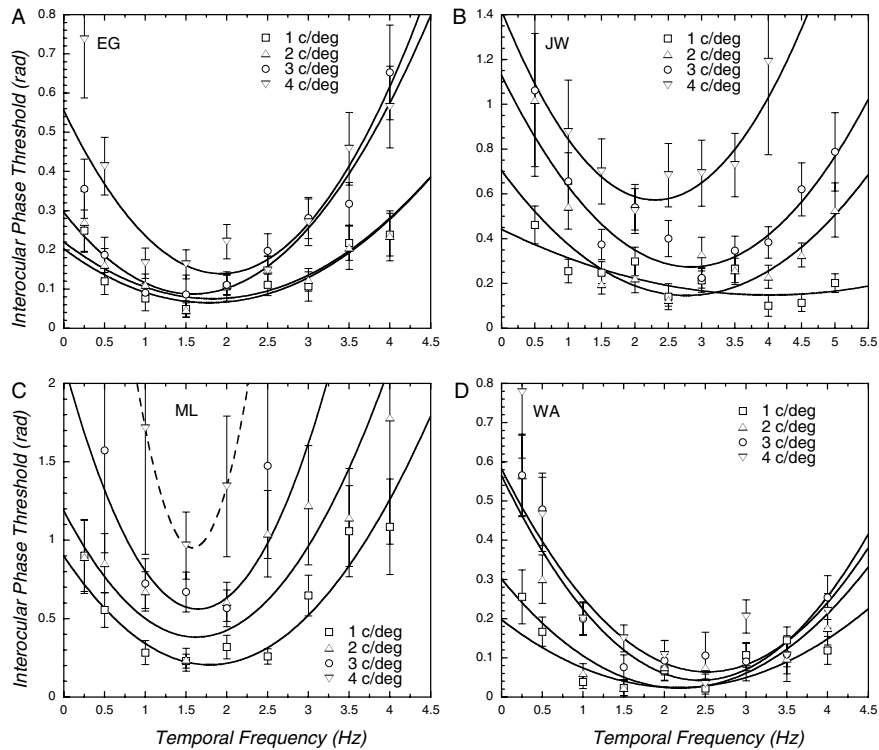


Fig. 5. Interoocular phase difference thresholds (radians) plotted against temporal frequency (Hz) for all four observers. In the unrestricted model  $\Theta_{12}$  a parabolic curve with three parameters is fitted to each data set. Error bars denote confidence intervals.

Table 1  
Unrestricted model with 12 parameters

Obs.	Spatial frequency (c/deg)	MLE $\Theta_{12}$			$\chi^2$ (12)	<i>p</i>
		Half-curv. <i>a</i>	Horiz. shift <i>b</i> (Hz)	Vert. shift <i>c</i> (rad)		
EG	1	2.48	1.78	0.065	17.8	0.88
	2	2.49	1.83	0.075		
	3	4.77	1.58	0.087		
	4	6.39	1.93	0.139		
JW	1	1.04	4.02	0.148	19.6	0.93
	2	4.16	2.77	0.146		
	3	6.07	2.84	0.274		
	4	9.12	2.31	0.572		
ML	1	12.4	1.79	0.206	10.3	0.11
	2	17.5	1.62	0.382		
	3	33.1	1.65	0.562		
	4 <sup>a</sup>	128	1.58	0.951		
WA	1	2.16	2.17	0.024	39.3	0.99
	2	3.32	2.19	0.023		
	3	5.03	2.43	0.042		
	4	4.65	2.53	0.064		

Maximum likelihood estimates (MLE  $\Theta_{12}$ ) of half-curvature *a*, horizontal shift *b* (expressed in Hz), and vertical shift *c* (expressed in rad) for each observer and spatial frequency.  $\chi^2$  values correspond to goodness-of-fit for discrimination thresholds measured in radians.

<sup>a</sup> Fit to three data points only.

conditions, giving a total of 12 degrees of freedom per observer (Table 1). Individual peak performances as measured by parameter *b* were typically obtained between 1.7 and 2.8 Hz (with one exception at 1 c/deg). Thresholds increased with spatial frequency systemati-

cally for observers ML and JW and to a lesser extent for observers EG and WA (see parameter *c* in Table 1).

In order to test whether tuning curves of each observer are temporal frequency tuned (i.e., centered on a single temporal frequency), we attempted to fit our data with

Table 2  
Restricted models with three parameters

Obs.	Phase MLE $\Theta_3$			$\chi^2(9)$	$p$	Disparity MLE $\Theta_3$			$\chi^2(9)$	$p$
	$a$	$b$ (Hz)	$c$ (rad)			$a$	$b$ (Hz)	$c$ (arcsec)		
EG	3.10	1.76	0.087	34.0	0.99***	15.4	1.76	20.2	15.6	0.93
JW	1.38	3.46	0.213	68.6	0.99***	17.8	2.93	55.5	19.6	0.98*
ML	12.4	1.83	0.290	28.3	0.99***	93.5	1.68	114.6	2.94	0.05
WA	3.29	2.25	0.027	33.2	0.99***	13.2	2.42	11.3	10.4	0.67

Maximum likelihood estimates (MLE) of half-curvature  $a$ , horizontal shift  $b$  (temporal frequency in Hz), and vertical shift  $c$  for interocular phase difference (rad) and for horizontal disparity (arcsec) for each observer.  $\chi^2$  values correspond to likelihood ratio tests of restricted versus unrestricted model.

\*Significant for  $\alpha = 0.05$ , \*\*\* $\alpha = 0.001$ .

models restricted to fewer degrees of freedom. The first restricted model  $\Theta_9$  assumes the same horizontal alignment (parameter  $b$ ) for each parabola giving a total of 9 degrees of freedom for each observer. The null hypothesis then states that a restricted model fits the individual data equally well. The ratio of the likelihoods for the two models are entered in the test statistic  $-2 \log \Lambda$  with  $\Lambda = \max\{lik(\Theta_9)\} / \max\{lik(\Theta_{12})\}$ . For large numbers this statistic is  $\chi^2$ -distributed with  $12 - 9 = 3$  degrees of freedom (e.g., Rice, 1988), and the point defining the upper 5% of the  $\chi^2(3)$  distribution is 7.81. Using this test, we could reject the hypothesis that peaks are horizontally aligned on the same temporal frequency only for observer JW (due to the 1 c/deg condition). A further restricted six-parameter model where a unique horizontal and vertical alignment were allowed per observer (parameters  $b$  and  $c$ ) could be rejected for both observers JW and ML.

Finally, we tested whether a single parabolic curve could fit the individual data sets equally well. Here the restricted model  $\Theta_3$  assumes a single half curvature, vertical and horizontal position (parameters  $a$ ,  $b$ , and  $c$ ) for the four spatial frequency conditions giving a total of 3 degrees of freedom. The hypothesis of a single parabola describing the temporal frequency tuning of interocular phase thresholds is violated for all four observers (see Table 2).

The increase of thresholds with spatial frequency for observers ML and JW is similar to that predicted by a model monitoring binocular horizontal disparity (see again Fig. 3C). We therefore converted thresholds in units of horizontal disparity and repeated the nested model hypothesis testing described above. The hypothesis of a single parabola describing the tuning curves for disparity thresholds holds for all observers with the exception of Observer JW (Table 2). In other words, spatial and temporal tuning is well described by a single parabolic curve if discrimination thresholds are expressed as disparity thresholds.

## 5. Discussion

Motion in depth is perceived for temporal frequencies of oscillation between 0.1 Hz and about 6 Hz and has

consistently been found to be worse than lateral motion (e.g., Beverley & Regan, 1974; Norcia & Tyler, 1984; Regan & Beverley, 1973a, 1973b; Richards, 1972). However, in these studies, spatial *and* temporal tuning characteristics of motion in depth remained relatively unspecified. In the present study, we determined the tuning characteristics for motion-in-depth perception with a variation of the Pulfrich effect. We designed our stimuli to keep control over their spatial and temporal frequency and chose a task that required discrimination of motion direction in depth. Discrimination thresholds consistently showed band-pass tuning in temporal frequency. Peaks of sensitivity were typically centered on values between 1.6 and 2.8 Hz and thresholds increased for temporal frequencies below 1.5 Hz and above 3–4 Hz. Temporal frequency tuning was independent of spatial frequency over a fourfold range of spatial frequency. There was however a systematic effect of spatial frequency in at least half of our observers, with thresholds increasing linearly with spatial frequency. In the remaining of this section, we discuss these results and the results of two additional experiments with respect to various models for motion in depth.

### 5.1. Models for motion in depth

Interocular phase difference, interocular delay, and maximal horizontal disparity are directly related to the three explanations of the Pulfrich effect. These explanations also feature in three basic models for the perception of motion in depth. (1) The *stereo-first* model assumes disparity encoding followed by binocular motion processing (e.g., Cumming, 1995; Cumming & Parker, 1994). In our task, such a model would first extract disparities and then compute change of disparity over time. (2) The *motion-first* model postulates monocular motion processing followed by stereo processing (e.g., Georgeson & Shackleton, 1989; Lu & Sperling, 1995; Regan, 1993; Regan & Beverley, 1979; Regan, Beverley, & Cynader, 1979). In our task, this model would monitor the sinusoidal monocular motion before binocular motion-stereo is established. (3) Finally, the *stereo-motion* model suggests joint encoding of binocu-

lar horizontal disparity and interocular delay (e.g., Burr & Ross, 1979; Morgan, 1979; Qian, 1994; Qian & Andersen, 1997). This model would attempt to encode monocular motion and binocular horizontal disparity simultaneously. We now discuss the plausibility of each of these models in turn.

### 5.2. Stereo-first

In this framework disparity encoding is the first step followed by the computation of disparity changes. The increase of discrimination thresholds with spatial frequency is consistent with such a framework (compare Figs. 3C and 5). It seems reasonable to assume that changing disparity over time will then be responsible for band-pass temporal frequency tuning. However, it is important to remember that a change in disparity alone does not reveal the motion direction in depth in this task. Therefore, for such a model to explain our data, motion signals would somehow need to be re-integrated with the change of disparities.

In an attempt to establish a baseline for the discrimination performance of the stereo system, we also measured thresholds for stationary Gabor patches at 1 c/deg. The same apparatus, stimuli, and procedure as in the main experiment were used. The task was to discriminate stimuli in front or behind the fixation cross. Although two observers (EG and ML) occasionally reported that they experienced depth, their responses were non-systematic. Fits of psychometric functions to the data were very poor and no reliable discrimination thresholds could be determined (results not shown). The present result is in line with earlier findings showing superior stereo acuity for motion in depth than for stereo processing alone (e.g., Schor, Wood, & Ogawa, 1984). It is unclear however why observers were so poor in this task as compared to the motion-in-depth task. What may have affected stereo acuity is the fact that in our setup, the fixation cross and envelope are the only relative disparity cues (McKee, Verghese, & Farell, 2001). Presumably a static stimulus with a single spatial frequency activates relatively few disparity detectors whereas a stimulus moving in depth introduces considerable pooling of activation across depth planes.

### 5.3. Motion-first

A motion-first system may respond to a temporal delay or a velocity difference between stimuli moving in the left and right eye. Previous findings indicate that perception of motion in depth is limited to interocular delays of up to 200–300 ms in dynamic noise patterns (e.g., Falk, 1980; Morgan & Ward, 1980; Ross, 1974). This threshold indicates an upper limit of temporal integration. There seems to be no lower limit when phase thresholds are expressed as temporal delay although

delay thresholds less than 300  $\mu$ s are neurophysiologically implausible (Morgan & Castet, 1995). In the present experiment, we predicted that monitoring interocular delays would produce a linear increase of thresholds with temporal frequency (Fig. 3B) but our data turned out to be band pass. Alternatively a motion-first system may track interocular velocity differences (e.g., Lu & Sperling, 1995; Regan & Beverley, 1979; Shioiri et al., 2000). We predicted that monitoring interocular velocity difference would produce a decrease of thresholds as temporal frequency increased (Fig. 3D), but again our data showed a peak in temporal frequency sensitivity.

In an attempt to establish a baseline for the discrimination performance of a system based primarily on interocular delay or velocity difference, we performed an additional experiment with horizontal gratings now moving in the *vertical* direction. We reasoned that such a system should be relatively insensitive to horizontal as well as vertical disparities as long as there is a detectable interocular delay. A similar apparatus and procedure as in the main experiment was used but with gratings oriented at 180° (horizontal) and moving sinusoidally up and down. In contrast to the main experiment an interocular phase difference introduced a vertical displacement but no horizontal offset. Observers had to discriminate upward from downward motion when the grating was moving in front of or behind the fixation plane. Discrimination performances of three observers (EG, ML, and WA) were measured for gratings with 1 c/deg oscillating at 1 Hz. Fits of Gaussian cumulative distribution functions to the data were very poor (results not shown). The Pulfrich effect is severely impaired, if not absent when interocular phase difference is unrelated to horizontal disparity. This result confirms earlier findings (Kolehmainen & Keskinen, 1974) suggesting that interocular delay and velocity difference, at least in the case of vertical motion, cannot reliably evoke perception of motion in depth.

### 5.4. Stereo-motion

Qian and Andersen (1997) developed a hybrid energy model that encodes motion and disparity energy in a unified framework. Activation of model complex cells in this motion-stereo model can explain the classical Pulfrich effect as well as most Pulfrich-like effects. Qian and Andersen derived from their model that the effect of a stimulus with interocular time delay  $T$  and disparity  $H$  on a complex cell with preferred phase difference  $\Delta\phi$ , horizontal spatial frequency  $\omega_x$ , and temporal frequency  $\omega_t$  approximates disparity activation  $d$  by

$$d \approx H + \frac{\omega_t}{\omega_x} T. \quad (9)$$

According to Eq. (9), a model complex cell will respond to interocular delay  $T$  as well as binocular horizontal

disparity  $H$  in a stimulus. As a consequence, the response of a disparity-selective complex cell may be caused by interocular temporal delay, binocular horizontal disparity or both. A crucial assumption of the model is that the most responsive cells in a population of uniformly distributed disparity-selective motion energy filters determine perceived motion in depth.

It is difficult to make predictions for our task from this hybrid energy model but Eq. (9) in connection with the assumption of a population of uniformly distributed spatial-, temporal-, and disparity-selective complex cells suggests constant phase thresholds as predicted in Fig. 3A. If we introduce the assumption that the population of disparity-selective motion energy filters has band-pass temporal resolution then it may be possible to reconcile Qian and Andersen's (1997) model with the present findings on temporal frequency tuning. In the light of spatial frequency dependency however, it seems more plausible that performance is limited by the temporal integration of disparity changes at a subsequent processing stage.

### 5.5. True encoding of motion in depth

Theoretically, true encoding of motion in depth can only occur when binocular cells have different motion preferences in the left and right eye. Tyler (1971) and later Westheimer (1990), both using line stimuli, reported that thresholds for detecting motion in depth are much higher than for detecting motion in the fronto-parallel plane. This agrees with the fact that most visual cortical cells have corresponding motion preferences in the two eyes (Ohzawa, DeAngelis, & Freeman, 1996, 1997) and are therefore not truly tuned to motion in depth (Spileers, Orban, Gulyas, & Maes, 1990). Maunsell and Van Essen (1983) also found no MT neurons that were truly tuned to motion in depth.

Cumming and Parker (1994) using dynamic random dot patterns concluded that motion in depth is primarily detected by means of temporal change of binocular disparity. Harris and Watamaniuk (1995), however, found that the rate of disparity change is not a good cue for speed discrimination of dynamic random-dot stereograms receding through zero disparity but their results may be valid under specific conditions only (Portfors-Yeomans & Regan, 1996). In any case disparity change alone is not sufficient to determine motion direction in depth. Sumnall and Harris (2002) reported detection and discrimination thresholds for a wide range of trajectories in depth that can be predicted by probability summation of independent mechanisms tuned to motion in the fronto-parallel and motion in the median plane of the head. This framework provides a possible explanation of results, although averaging and subtracting of velocities from the left and right eye and subsequent re-integration appears somewhat cumbersome.

### 5.6. Directions for future research

The main result of our experiment is the band-pass tuning in temporal frequency of the discrimination thresholds. None of the simple predictions we presented could account for this tuning. In particular, we can reject models that would monitor only interocular phase, interocular delays, binocular disparities or interocular velocity differences. A system that integrates disparity and delay simultaneously would have access to motion direction in depth but requires additional assumptions to explain band-pass temporal tuning and spatial frequency dependence. The band-pass tuning in temporal frequency is likely to be the result of an optimal temporal integration window that monitors changes in disparity over time. Future studies should be directed to elucidate the characteristics of this integration window.

## 6. Conclusions

We have designed a modified Pulfrich experiment to investigate the spatial and temporal limits of perceiving motion direction in depth. We found that discrimination thresholds were smallest for temporal frequencies near 2 Hz and increased with spatial frequency. Removal of either motion or disparity led to a breakdown of disparity and motion-in-depth perception, respectively. These results point to a stereo-motion system that monitors disparity and motion with limited temporal resolution.

### Acknowledgements

This research was funded by the Engineering and Physical Science Research Council UK (to ML), Human Frontier SP (to PM), and NSF-IRFP (to EG). Parts of this paper were presented at VSS 2002 in Sarasota, FL. We are grateful for valuable comments by two anonymous referees.

### Appendix A. Stimulus properties

Our stimulus is defined by a sinusoidal carrier presented to each eye (see Eq. (1)). In particular, the carrier of the left image is defined as

$$I_l(x, t) = \cos\{\omega_x x + \sin(\omega_t t + \phi/2)\}, \quad (\text{A.1})$$

where  $\omega_x$  is the angular spatial frequency with units in radians per degree visual angle (rad/deg) and  $\omega_t$  is the angular temporal frequency (in rad/s). The carrier for the right image is similarly defined with opposite phase. The spatial period of the carrier  $\Delta x$  is such that  $I_l(x, t) = I_l(x + \Delta x, t)$  and equals

$$\Delta x = \frac{2\pi}{\omega_x} = \frac{1}{f_x}, \quad (\text{A.2})$$

where  $f_x$  is the spatial frequency with units in cycles per degree visual angle (c/deg). Similarly, the temporal period  $\Delta t$  is such that  $I_l(x, t) = I_l(x, t + \Delta t)$  and equals

$$\Delta t = \frac{2\pi}{\omega_t} = \frac{1}{f_t}, \quad (\text{A.3})$$

where  $f_t$  is the temporal frequency (in c/s).

When  $x = 2k\pi/\omega_x$  ( $k \in \mathbf{N}$ ), the luminance profile over time can be approximated by

$$I(x, t) \approx \frac{3}{4} + \frac{1}{4} \cos(2\omega_t t + \phi), \quad (\text{A.4})$$

which is sinusoidal with temporal frequency  $2f_t$ . For other values of  $x$ , the temporal variation of luminance tends to be non-sinusoidal.

#### A.1. Interocular phase difference

Interocular phase difference  $\Delta\phi$  (in radians) is defined as the phase difference between the two monocular images and is therefore simply

$$\Delta\phi = +\phi/2 - (-\phi/2) = \phi. \quad (\text{A.5})$$

It is clear that this measure is independent of spatial and temporal frequency.

#### A.2. Interocular temporal delay

The interocular temporal delay  $T$  (in seconds) is the time needed for the luminance in the left and right images to coincide for any position, i.e.,  $I_l(x, t) = I_r(x, t + T)$ . This interocular temporal delay is therefore

$$T = \frac{\phi}{\omega_t}. \quad (\text{A.6})$$

Interocular delay is a measure that depends on temporal frequency but is independent of spatial frequency.

#### A.3. Binocular horizontal disparity

The binocular horizontal disparity  $H$  (in degrees of visual angle) is the spatial offset between the left and right images, i.e.  $I_l(x, t) = I_r(x + H, t)$ . Disparity varies with time:

$$\begin{aligned} H(t) &= \frac{1}{\omega_x} [\sin(\omega_t t + \phi/2) - \sin(\omega_t t - \phi/2)] \\ &= \frac{2}{\omega_x} \cos(\omega_t t) \sin(\phi/2). \end{aligned} \quad (\text{A.7})$$

Disparity is therefore dependent on both spatial and temporal frequency. The maximal disparity can be

found by nulling the derivative of disparity. The derivative is given by

$$H'(t) = -2 \frac{\omega_t}{\omega_x} \sin(\omega_t t) \sin(\phi/2). \quad (\text{A.8})$$

For  $t = k\pi/\omega_t$  ( $k \in \mathbf{N}$ ) the derivative  $H'(t) = 0$  and  $H(t)$  has extrema equal to  $\pm 2 \sin(\phi/2)/\omega_x$ . For the range of phases in our experiment ( $-\pi/3 < \phi < +\pi/3$ ), the maximal horizontal disparity is well approximated by

$$H_{\max} \approx \frac{\phi}{\omega_x}. \quad (\text{A.9})$$

Thus maximal disparity depends on spatial frequency but not on temporal frequency. Note that the maximal disparity becomes just  $\phi$  when expressed as spatial phase difference (in radians). In other words, maximal spatial phase difference equals interocular phase difference as defined in Appendix A.1.

#### A.4. Interocular velocity difference

In order to compute the image velocity, we need to differentiate the carrier with respect to time and space:

$$\begin{cases} \frac{\partial I_l(x, t)}{\partial t} = -\omega_t \cos(\omega_t t + \phi/2) \sin\{\omega_x x + \sin(\omega_t t + \phi/2)\}, \\ \frac{\partial I_l(x, t)}{\partial x} = -\omega_x \sin\{\omega_x x + \sin(\omega_t t + \phi/2)\}. \end{cases} \quad (\text{A.10})$$

The left image velocity  $v_l$  (in deg/s) is then given by

$$v_l = -\frac{\partial I_l(x, t)/\partial t}{\partial I_l(x, t)/\partial x} = -\frac{\omega_t}{\omega_x} \cos(\omega_t t + \phi/2), \quad (\text{A.11})$$

with extrema of  $v_l$  equal to  $\pm\omega_t/\omega_x$  at  $t = (k\pi - \phi/2)/\omega_t$  ( $k \in \mathbf{N}$ ) and  $\omega_t, \omega_x > 0$ . A similar expression can be found for the velocity in the right image. The velocity difference  $U$  between the left and right images is then

$$\begin{aligned} U(t) &= -\frac{\omega_t}{\omega_x} [\cos(\omega_t t - \phi/2) - \cos(\omega_t t + \phi/2)] \\ &= -2 \frac{\omega_t}{\omega_x} \sin(\omega_t t) \sin(\phi/2). \end{aligned} \quad (\text{A.12})$$

The extrema of velocity difference are obtained by nulling the derivative of  $U(t)$ .

$$U'(t) = 2 \frac{\omega_t}{\omega_x} \sin(\omega_t t) \sin(\phi/2). \quad (\text{A.13})$$

These extrema are found for  $t = (\pi/2 + k\pi)/\omega_t$  ( $k \in \mathbf{N}$ ) and they equal  $\pm 2 \sin(\phi/2)(\omega_t/\omega_x)$ . Maximal velocity difference therefore depends on spatial and temporal frequency and is approximated by

$$U_{\max} \approx \phi \frac{\omega_t}{\omega_x}. \quad (\text{A.14})$$

When comparing Eqs. (A.7) and (A.12), it becomes obvious that interocular velocity difference is maximal when horizontal disparity is zero and disparity is maximal when velocity difference is zero (see Fig. 6). Note

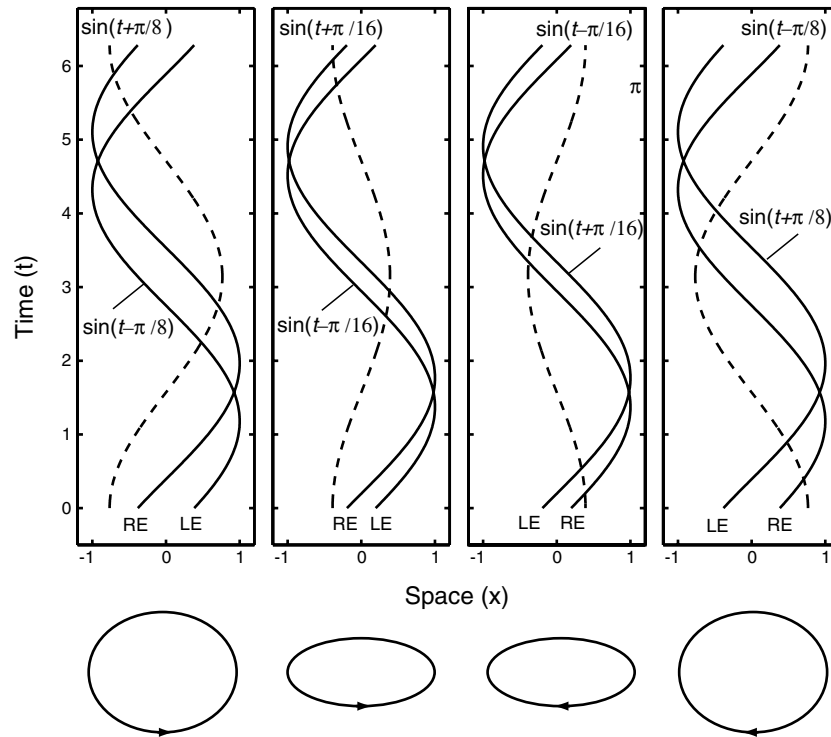


Fig. 6. Space–time plots of sinusoidal motions in the left and right eye. The four panels show sinusoidal motion (solid lines) with phase difference  $+\pi/4$ ,  $+\pi/8$ ,  $-\pi/8$ , and  $-\pi/4$  between the left and the right eye and corresponding horizontal disparity modulations (dashed lines). Perceived elliptical paths and direction of motion in depth are illustrated below each panel.

also that Eqs. (A.8) and (A.12) indicate that rate of disparity change and velocity difference are equivalent.

## References

- Adelson, E. H., & Bergen, J. R. (1985). Spatio-temporal energy models for the perception of motion. *Journal of the Optical Society of America A*, 2, 284–299.
- Albright, T. D. (1984). Direction and orientation selectivity of neurons in visual area MT of the macaque. *Journal of Neurophysiology*, 52, 1106–1130.
- Anzai, A., Ohzawa, I., & Freeman, R. D. (2001). Joint encoding of motion and depth by visual cortical neurons: neural basis of the Pulfrich effect. *Nature Neuroscience*, 4, 513–518.
- Beverley, K. I., & Regan, D. (1974). Temporal integration of disparity information in stereoscopic perception. *Experimental Brain Research*, 19, 228–232.
- Brainard, D. D. (1997). The psychophysics toolbox. *Spatial Vision*, 10, 433–436.
- Burr, D. C., & Ross, J. (1979). How does binocular delay give information about depth? *Vision Research*, 19, 523–532.
- Carney, T., Paradiso, M. A., & Freeman, R. D. (1989). A physiological correlate of the Pulfrich effect in cortical neurons of the cat. *Vision Research*, 29, 155–165.
- Cumming, B. G. (1995). The relationship between stereoacuity and stereomotion thresholds. *Perception*, 24, 105–114.
- Cumming, B. G., & Parker, A. J. (1994). Binocular mechanisms for detecting motion-in-depth. *Vision Research*, 34, 483–496.
- Cynader, M. S., & Regan, D. (1978). Neurons in cat parastriate cortex sensitive to the direction of motion in three-dimensional space. *Journal of Physiology (London)*, 274, 549–569.
- Cynader, M. S., & Regan, D. (1982). Neurons in cat visual cortex tuned to the direction of motion in depth: effect of positional disparity. *Vision Research*, 22, 967–982.
- Falk, D. S. (1980). Dynamic visual noise and the stereophenomenon: inter-ocular time delays, depth and coherent velocities. *Perception & Psychophysics*, 28, 19–27.
- Felleman, D. J., & Van Essen, D. C. (1987). Receptive field properties of neurons in area V3 of macaque monkey extrastriate cortex. *Journal of Neurophysiology*, 57, 889–920.
- Fleet, D. J., Wagner, A., & Heeger, D. J. (1996). Encoding of binocular disparity: energy models, position shifts and phase shifts. *Vision Research*, 36, 1839–1858.
- Georgeson, M. A., & Shackleton, T. M. (1989). Monocular motion sensing, binocular motion perception. *Vision Research*, 32, 193–198.
- Harris, J. M., & Watamaniuk, S. N. J. (1995). Speed discrimination of motion-in-depth using binocular cues. *Vision Research*, 35, 885–896.
- Howard, I. P., & Rogers, B. J. (2002). *Seeing in depth* (Vol. 2). Toronto: I. Porteous, Toronto University Press.
- Hubel, D. H., & Wiesel, T. (1968). Receptive fields and functional architecture of the monkey striate cortex. *Journal of Physiology*, 195, 215–243.
- Julesz, B., & White, B. (1969). Short term visual memory and the Pulfrich phenomenon. *Nature*, 222, 639–641.
- Kaufman, D. A., & Palmer, L. A. (1990). The luminance dependence of spatiotemporal response of cat striate cortical units. *Investigative Ophthalmology and Visual Science*, 31, S398.
- Kolehmainen, K., & Keskinen, E. (1974). Evidence for the latency-time explanation of the Pulfrich phenomenon. *Scandinavian Journal of Psychology*, 15, 320–321.
- Lee, D. N. (1970). A stroboscopic stereophenomenon. *Vision Research*, 10, 587–593.
- Lu, Z.-L., & Sperling, G. (1995). The functional architecture of human visual motion perception. *Vision Research*, 35, 2697–2722.

- Marr, D., & Ullman, C. (1981). Directional selectivity and its use in early visual processing. *Proceedings of the Royal Society of London, B*, 211, 187–217.
- Maunsell, J. H. R., & Van Essen, D. C. (1983). Functional properties of neurons in middle temporal visual area of the Macaque monkey II. Binocular interactions and sensitivity to binocular disparity. *Journal of Neurophysiology*, 49, 1148–1167.
- McKee, S. P., Verghese, P., & Farell, B. (2001). Sinusoidal gratings at multiple scales to resolve depth ambiguity. *Investigative Ophthalmology and Visual Science*, 42, S938.
- Morgan, M. J. (1975). Stereo-illusion based on visual persistence. *Nature (London)*, 256, 639–640.
- Morgan, M. J. (1979). Perception of continuity in stroboscopic motion: a temporal frequency analysis. *Vision Research*, 19, 491–500.
- Morgan, M. J., & Castet, E. (1995). Stereoscopic depth perception at high velocities. *Nature (London)*, 378, 380–383.
- Morgan, M. J., & Fahle, M. (2000). Motion-stereo mechanisms sensitive to inter-ocular phase. *Vision Research*, 40, 1667–1675.
- Morgan, M. J., & Thompson, P. (1975). Apparent motion and the Pulfrich effect. *Perception*, 4, 3–18.
- Morgan, M. J., & Ward, R. (1980). Interocular delay produces depth in subjectively moving noise patterns. *Quarterly Journal of Experimental Psychology*, 32, 387–395.
- Norcia, A. M., & Tyler, C. W. (1984). Temporal frequency limits for stereoscopic apparent motion processes. *Vision Research*, 4, 395–401.
- Ohzawa, I. (1998). Mechanisms of stereoscopic vision: the disparity energy model. *Current Opinion in Neurobiology*, 8, 509–515.
- Ohzawa, I., DeAngelis, G. C., & Freeman, R. D. (1996). Encoding of binocular disparity by simple cells in the cat's visual cortex. *Journal of Neurophysiology*, 75, 1779–1805.
- Ohzawa, I., DeAngelis, G. C., & Freeman, R. D. (1997). Encoding of binocular disparity by complex cells in the cat's visual cortex. *Journal of Neurophysiology*, 77, 2879–2909.
- Pack, C. C., Born, R. T., & Livingstone, M. S. (2003). Two-dimensional substructure of stereo and motion interactions in macaque visual cortex. *Neuron*, 37, 525–535.
- Pelli, D. G. (1997). The videotoolbox software for visual psychophysics: Transferring numbers into movies. *Spatial Vision*, 10, 437–442.
- Pettigrew, J. D. (1973). Binocular neurons which signal change of disparity in area 18 of cat visual cortex. *Nature—New Biology*, 241, 123–124.
- Poggio, G. F., & Fischer, B. (1977). Binocular interaction and depth sensitivity in striate and prestriate cortex of behaving rhesus monkey. *Journal of Neurophysiology*, 40, 1392–1405.
- Poggio, G. F., & Talbot, W. H. (1981). Mechanisms of static and dynamic stereopsis in foveal cortex of the rhesus monkey. *Journal of Physiology (London)*, 315, 469–492.
- Portfors-Yeomans, & Regan, D. (1996). Cyclopean discrimination thresholds for the direction and speed of motion in depth. *Vision Research*, 36, 3265–3279.
- Pulfrich, C. (1922). Die Stereoskopie im Dienste der isochromen und heterochromen Photometrie. *Naturwissenschaften*, 10, 553–564.
- Qian, N. (1994). Computing stereo disparity and motion with known binocular cell properties. *Neural Computations*, 6, 390–404.
- Qian, N., & Andersen, R. A. (1997). A physiological model for motion-stereo integration and a unified explanation of Pulfrich-like phenomena. *Vision Research*, 37, 1683–1698.
- Reichardt, W. (1961). Autocorrelation, a principle for the evaluation of sensory information by the central nervous system. In W. A. Rosenblith (Ed.), *Sensory communication*. New York: Wiley.
- Regan, D. (1993). Binocular correlates of the direction of motion in depth. *Vision Research*, 33, 2359–2360.
- Regan, D., & Beverley, K. I. (1973a). Some dynamic features of depth perception. *Vision Research*, 13, 2369–2379.
- Regan, D., & Beverley, K. I. (1973b). The dissociation of sideways movement from movement in depth: psychophysics. *Vision Research*, 13, 2403–2415.
- Regan, D., & Beverley, K. I. (1979). Binocular and monocular stimuli for motion in depth: changing disparity and changing size feed the same motion-in-depth stage. *Vision Research*, 19, 1331–1342.
- Regan, D., Beverley, K. I., & Cynader, M. (1979). Separate subsystems for position in depth and for motion in depth. *Proceedings of the Royal Society of London B*, 204, 485–501.
- Rice, J. A. (1988). *Mathematical statistics and data analysis*. Belmont, CA: Wadsworth and Brooks.
- Richards, W. (1972). Response functions for sine- and square-wave modulations of disparity. *Journal of the Optical Society of America*, 62, 907–911.
- Rogers, B. J., & Anstis, S. M. (1972). Intensity versus adaptation and the Pulfrich stereophenomenon. *Vision Research*, 12, 909–928.
- Ross, J. (1974). Stereopsis by binocular delay. *Nature (London)*, 248, 363–364.
- Ross, J., & Hogben, J. H. (1975). The Pulfrich effect and short-term memory in stereopsis. *Vision Research*, 15, 1289–1290.
- Sanger, T. D. (1988). Stereo disparity computation using Gabor filters. *Biological Cybernetics*, 59, 405–418.
- Schor, C. M., Wood, I. C., & Ogawa, J. (1984). Spatial tuning of static and dynamic local stereopsis. *Vision Research*, 24, 573–578.
- Shioiri, S., Saisho, H., & Yaguchi, H. (2000). Motion in depth based on inter-ocular velocity differences. *Vision Research*, 40, 2565–2572.
- Spileers, W., Orban, G. A., Gulyas, B., & Maes, H. (1990). Selectivity of cat area 18 neurons for direction and speed in depth. *Journal of Neurophysiology*, 63, 936–954.
- Sumnall, J. H., & Harris, J. M. (2002). Minimum displacement thresholds for binocular three-dimensional motion. *Vision Research*, 42, 715–724.
- Tyler, C. (1971). Stereoscopic depth movement: two eyes less sensitive than one. *Science*, 174, 958–961.
- Tyler, C. (1974). Stereopsis in dynamic visual noise. *Nature*, 250, 781–782.
- Van Santen, J. P. H., & Sperling, G. (1985). Elaborated Reichardt detectors. *Journal of the Optical Society of America A*, 2, 300–321.
- Watson, A. B., & Ahumada, A. J., Jr. (1985). Model of human visual motion sensing. *Journal of the Optical Society of America A*, 2, 322–342.
- Westheimer, G. (1990). Detection of disparity motion by the human observer. *Ophthalmology and Vision Science*, 67, 627–630.
- Wichmann, F. A., & Hill, N. J. (2001a). The psychometric function I: fitting, sampling, and goodness-of-fit. *Perception & Psychophysics*, 63, 1293–1313.
- Wichmann, F. A., & Hill, N. J. (2001b). The psychometric function II: bootstrap based confidence intervals and sampling. *Perception & Psychophysics*, 63, 1314–1329.